

SPECTRAL DECOMPOSITION OF ATOMIC STRUCTURES IN HETEROGENEOUS CRYO-EM

CARLOS ESTEVE-YAGÜE, WILLEM DIEPEVEEN, OZAN ÖKTEM, AND CAROLA-BIBIANE SCHÖNLIEB

ABSTRACT. We consider the problem of recovering the three-dimensional atomic structure of a flexible macromolecule from a heterogeneous cryo-EM dataset. The dataset contains noisy tomographic projections of the electrostatic potential of the macromolecule, taken from different viewing directions, and in the heterogeneous case, each image corresponds to a different conformation of the macromolecule. Under the assumption that the macromolecule can be modelled as a chain, or discrete curve (as it is for instance the case for a protein backbone with a single chain of amino-acids), we introduce a method to estimate the deformation of the atomic model with respect to a given conformation, which is assumed to be known a priori. Our method consists on estimating the torsion and bond angles of the atomic model in each conformation as a linear combination of the eigenfunctions of the Laplace operator in the manifold of conformations. These eigenfunctions can be approximated by means of a well-known technique in manifold learning, based on the construction of a graph Laplacian using the cryo-EM dataset. Finally, we test our approach with synthetic datasets, for which we recover the atomic model of two-dimensional and three-dimensional flexible structures from noisy tomographic projections.

1. INTRODUCTION

One of the central problems in the field of structural biology is that of determining the three-dimensional structure and dynamics of biological macromolecules. It is well-known that the function of biological macromolecules is determined, not only by the chemical composition, but also by the three-dimensional structure. Big macromolecules, such as proteins, can be composed of thousands of atoms and, despite of the physical and biological knowledge about the formation of the bonds between atoms, determining the three-dimensional configuration of big macromolecules turns out to be an extremely complex task. Moreover, most of these biological macromolecules are flexible and may deform their structure, adopting different conformations. In this case, providing a single

(Carlos Esteve-Yagüe, Willem Diepeveen and Carola-Bibiane Schönlieb) DEPARTMENT OF APPLIED MATHEMATICS AND THEORETICAL PHYSICS, UNIVERSITY OF CAMBRIDGE, UNITED KINGDOM.

(Ozan Öktem) DEPARTMENT OF MATHEMATICS, KTH, STOCKHOLM, SWEDEN.

E-mail addresses: `ce423@cam.ac.uk`, `wd292@cam.ac.uk`, `ozan@kth.se`, `cbs31@cam.ac.uk`.

Date: September 14, 2022.

Acknowledgements: The authors acknowledge support from the Alan Turing Institute for the project "Molecular structure from images under physical constraints". O. Öktem was partially supported by the Swedish Research Council Grant 2020-03107. C.B. Schönlieb acknowledges support from the Philip Leverhulme Prize, the Royal Society Wolfson Fellowship, the EPSRC advanced career fellowship EP/V029428/1, EPSRC grants EP/S026045/1 and EP/T003553/1, EP/N014588/1, EP/T017961/1, the Wellcome Innovator Awards 215733/Z/19/Z and 221633/Z/20/Z, the European Union Horizon 2020 research and innovation programme under the Marie Skłodowska-Curie grant agreement No. 777826 NoMADS, the Cantab Capital Institute for the Mathematics of Information and the Alan Turing Institute.

conformation of the macromolecule does not solve the problem of determining the three-dimensional structure, as one would like to provide a full description of all the possible conformations.

In single particle cryogenic electron microscopy (cryo-EM), an aqueous solution containing the macromolecule of interest is rapidly frozen and then imaged by means of a transmission electron microscope. Each image (micrograph) contains many samples of the macromolecule (particles) at various (unknown) conformations. During the process known as particle picking, the particles are individually selected from the micrograph to produce a series of two-dimensional images, each containing the tomographic projection of the electrostatic potential generated by the single particle and its surrounding buffer. The fact that the molecular sample may contain different conformations of the macromolecule makes single-particle cryo-EM a well-suited experimental technique to study the structural dynamics of the macromolecule.

The image formation in cryo-EM is typically modelled as a parallel beam ray transform (tomographic projection) of the function representing the electrostatic potential of the particle and surrounding buffer along a particular unknown viewing direction. This is followed by a two-dimensional convolution in the detector plane with a point spread function, which models the microscope optics and detector response. To formalise the above, let $\{u_1, \dots, u_n\}$ denote the functions representing the electrostatic potential of each of the particles in the molecular sample. Note that u_i can be viewed as a volumetric density function depending on the specific conformation and the orientation of each particle. The corresponding cryo-EM images $\{Y_1, \dots, Y_n\} \subset \mathbb{R}^{N \times N}$ can be modelled¹ as

$$(1.1) \quad Y_i = h_i * T(u_i) + \xi_i$$

where $h_i \in L^2(\mathbb{R}^2)$ is the so-called *point spread function* (PSF) and T is the parallel beam ray transform taken along the microscope optical axis. Here, ξ_i is taken from $(N \times N)$ -dimensional normal distribution, with $N \times N$ denoting the resolution in pixels of the 2D cryo-EM images. A detailed description of the image formation in cryo-EM can be found in [7, 30]. It is worth noting that, in order to avoid the damage of the molecular structure, the electron dose of the microscope is kept very low, resulting in micrographs dominated by noise (see Figure 1).

1.1. Related work. As already indicated, the goal in single particle cryo-EM is to recover the three-dimensional structure of a macromolecule from noisy tomographic projections of single particles, with the difficulty of not knowing the orientation of the particle in each projection. This problem has attracted a lot of attention in the last decade, and many methods have been proposed to address it, most of them under the assumption of having an homogeneous sample [7, 3, 6, 16, 28], where all the tomographic projections in the dataset are generated by particles with identical three-dimensional structure, i.e. the macromolecule has a single conformation. The prevalent method nowadays is the Bayesian approach introduced in [24], in which a probability distribution for the viewing directions of the tomographic projections and the density function producing these projections are estimated in an alternating manner. However, large macromolecules tend to be flexible, and therefore, the homogeneity assumption does not hold in those cases. Some methods have been proposed in the last years to recover the structural heterogeneity of macromolecules from single particle cryo-EM data. Here, we must make a distinction between two types of heterogeneity, namely,

¹We do not include the rotation and the spatial translation of the particle density in the forward operator, as it is usual in the cryo-EM literature. As we will see in the sequel, it is more convenient for us to assume that the orientation and the spatial location of the particle, as well as its specific conformation, are encoded in the particle density function u_i .

discrete heterogeneity, in which the molecular sample contains a small number of different conformations (typically two or three); and continuous heterogeneity, in which the three-dimensional structure varies continuously, and the conformations found in the molecular sample can be seen as an approximation of a continuous low-dimensional manifold. For the case of discrete heterogeneity, there are several software packages available, such as RELION [25], cryoSPARC [21], FREALIGN [15] and cisTEM [8], which classify the 2D cryo-EM images in clusters depending on the conformation and estimate the 3D electrostatic potential corresponding to each cluster.

For the case of continuous heterogeneity, which is the one that we address in this work, an existing approach consists in performing a Principal Component Analysis (PCA) of the 3D electrostatic potentials, represented in an $N' \times N' \times N'$ voxel grid [18, 19, 20, 14], with typically $N' \ll N$. See also the more recent works [12, 1, 2] for a variant of this method, which has shown to be able to recover the continuous heterogeneity in some molecular samples. However, as discussed in [17, subsection 3.3], this method is limited to low-resolution reconstructions of the three-dimensional structure. More recent works address the continuous heterogeneity by using Deep Neural Networks. For instance, CryoDRGN [31] uses a Variational Auto-Encoder (VAE) to estimate the density map corresponding to each conformation in the heterogeneous cryo-EM dataset. This is further developed in [23], which uses a VAE approach to recover the continuous heterogeneity, with the aim of reconstructing, not the volume density, but the atomic model associated to each conformation.

In [17], an interesting method based on manifold learning is proposed to increase the resolution of three-dimensional reconstructions of continuously heterogeneous macromolecules. Their idea consists in using the low-resolution density representation of the particles (obtained for instance by the methods in [2]) to construct a graph Laplacian, which is then used in lieu of the Laplace-Beltrami operator to approximate the spectral properties of the manifold of conformations \mathcal{M} . Then, a high-resolution volumetric voxel representation of the three-dimensional structure is estimated as a linear combination of the eigenvectors associated to the smallest eigenvalues of the graph Laplacian. The coefficients in the spectral decomposition of each voxel are estimated by solving a least squares problem, using the forward operator applied to the reconstructed densities, and comparing it with the noisy images in the dataset. These coefficients give a three-dimensional density map associated to each of the first eigenvalues that, in [17], are referred to as eigenvolumes.

1.2. Our contribution. In this work, we propose a variant of the method introduced in [17] to address the problem of recovering the three-dimensional structure in a heterogeneous cryo-EM dataset. The main difference with respect to [17] is that, instead of estimating a volumetric representation of the molecular structure, we rather aim at recovering the atomic model corresponding to each conformation, i.e. the three-dimensional configuration of the atoms conforming the macromolecule. In order to apply our method we need to make two important assumptions concerning the prior knowledge about the molecular structure:

- (i) We consider that the molecular structure is composed by a fixed number of atoms forming a chain, or discrete curve, in which the distance between adjacent atoms is constant.
- (ii) We assume that we have access to the atomic model of the macromolecule corresponding to a specific conformation.

Regarding the first assumption, although most of the macromolecules have more complex structures, many of them, as for instance proteins, can be approximated by means of a discrete curve

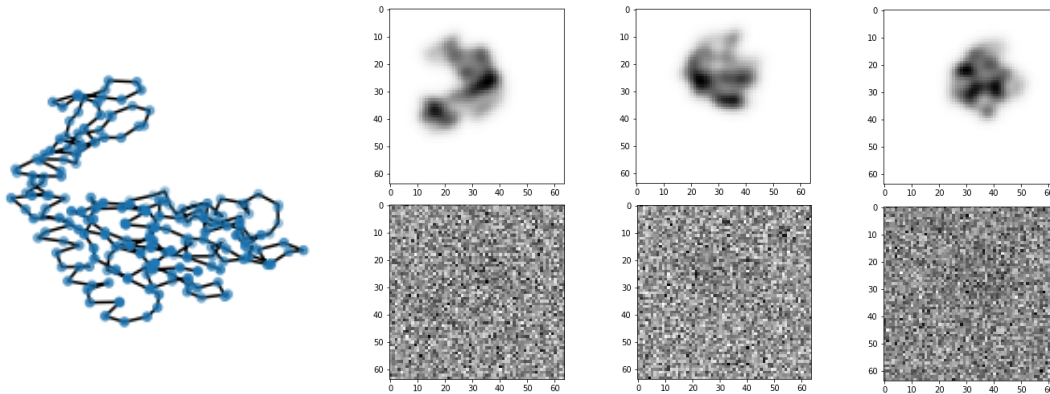


FIGURE 1. At the left we see the atomic model of the macromolecule in a specific conformation. At the right, we see the tomographic projections of the 3D electrostatic potential of three particles from different viewing directions and different conformations. The images in the first row are the clean images, and the images in the second row are the same images after the addition of Gaussian noise.

determining only the positions of the C- α atoms (see Remark 1.1). As for the second assumption, the atomic model for many macromolecules is available in existent databases. For the particular case of proteins, the recently developed deep learning based approach AlphaFold [11, 26, 27] can provide highly accurate predictions of the 3D structure of proteins from their primary sequence (sequence of amino-acids). However, the structures in the databases typically contain the information regarding the macromolecule in a single conformation. In this work, our goal is, indeed, to use the cryo-EM data to estimate the deformation of the atomic model in each particle of the molecular sample with respect to the known conformation (see Figure 2).

Remark 1.1. *An atomic model in which the atoms form a discrete curve can be used in practice as an approximation of the three-dimensional structure of a protein with a single chain of amino-acids. A protein is a macromolecule structure consisting of one or more chains of amino-acid residues, which are connected by peptide bonds, forming the so-called backbone. The central atom in each amino-acid residue is known as the C- α atom, and connects the side chain of the amino-acid residue to the backbone. One way to approximate the three-dimensional structure of the protein is by determining the C- α positions conforming the backbone, which form, indeed, a discrete curve satisfying our assumption [10].*

In the following, we offer a more formal description of our approach. See Figure 3 for a diagram outlining our method. The main idea is to use the prior knowledge about the molecular structure to introduce a parametrization of the space of atomic models satisfying such a prior, in our case, the assumption that the molecular structure can be modelled as a discrete curve. As we will see in subsection 2.1, such three-dimensional structures can be represented, up to translations and rotations, by the *torsion* and *bond* angles at each point of the discrete curve, that we denote by $\Theta = (\theta_1, \theta_2, \dots)$ and $\Psi = (\psi_1, \psi_2, \dots)$ respectively. In order to determine the conformation of the

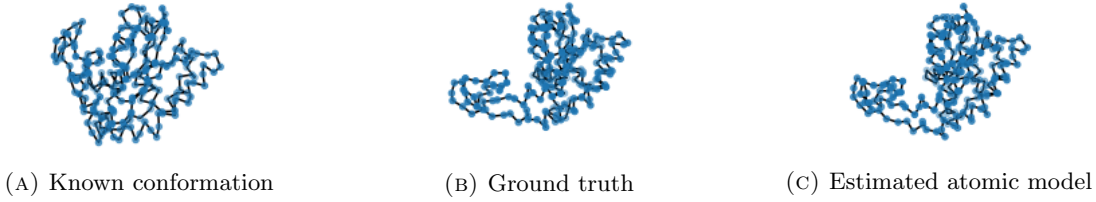


FIGURE 2. At the left, the atomic model of the known conformation, which is used as initial guess for all the particles. In the middle, the specific conformation of one of the particles of the synthetic dataset. At the right, the atomic model estimated by means of our method.

macromolecule for each particle u_i , we estimate the parameters Θ_i and Ψ_i as

$$(1.2) \quad \Theta_i = \Theta_i(A) := \Theta_0 + \sum_{k=0}^{K-1} \mathbf{a}_k \phi_i^{(k)} \quad \text{and} \quad \Psi_i = \Psi_i(B) := \Psi_0 + \sum_{k=0}^{K-1} \mathbf{b}_k \phi_i^{(k)},$$

where the vectors Θ_0 and Ψ_0 represent the torsion and bond angles of the atomic model in the known conformation, and the coefficient matrices $A = [\mathbf{a}_0, \mathbf{a}_1, \dots, \mathbf{a}_{K-1}]$ and $B = [\mathbf{b}_0, \mathbf{b}_1, \dots, \mathbf{b}_{K-1}]$ are to be estimated from the noisy cryo-EM images. Following the same ideas as in [17], the vectors $\{\phi^{(k)}\}_{k=0}^{K-1}$ defined as

$$\phi^{(k)} = \left(\phi_1^{(k)}, \phi_2^{(k)}, \dots, \phi_n^{(k)} \right) \in \mathbb{R}^n \quad \forall k \in \{0, 1, \dots, K-1\}$$

that we use in (1.2) are the eigenvectors associated to the K smallest eigenvalues of a graph Laplacian matrix, which is used to approximate the spectral properties of the unknown manifold of conformations \mathcal{M} (see Figures 4 and 12 for an illustration). As introduced in [17], this graph Laplacian can be constructed from a low-dimensional reconstruction of the particles. See subsection 2.1 for further details on the spectral decomposition of the atomic model, and appendix B for a description of the method to construct the graph Laplacian and the vectors $\phi^{(k)}$.

The number $K \in \mathbb{N}$ of eigenvectors in the spectral decomposition is a hyper-parameter that can be chosen depending on the flexibility of the structure, or the type of deformations that we aim to recover. Since we use only the terms in the spectral decomposition associated to the smallest eigenvalues of the graph Laplacian, our method is able to capture only the low-frequency deformations of the molecular structure. The deformations of high frequency, typically associated to small vibrations of the atoms, are not recovered by our method (see Remark 2.2). In our numerical experiments in section 3 we have used $K = 10$ and $K = 20$ respectively.

Finally, we need to estimate the coefficients \mathbf{a}_k and \mathbf{b}_k in the spectral decomposition (1.2). This is done in subsection 2.3 by means of a minimization problem, evaluating the data fidelity of the estimated atomic model for each particle with the corresponding cryo-EM image. Under the assumption that the molecular structure can be described as a discrete curve in \mathbb{R}^3 , and that the spatial location and orientation of the particles, represented by $\{(\hat{z}_i, \hat{F}_i)\}_{i=1}^n \in [\mathbb{R}^3 \times SO(3)]^n$, are

known², we estimate the 3D density associated to the i -th particle as a sum of Gaussian densities centred at the positions of the atoms in the i -th particle, i.e.

$$x \in \mathbb{R}^3 \mapsto \hat{U}_i(A, B)(x) = \sum_{z \in \Gamma_i(A, B)} \nu \exp \left[-\frac{\|x - z\|^2}{2\sigma^2} \right],$$

where $\nu, \sigma > 0$ are hyperparameters to be chosen a priori, and $\Gamma_i(A, B) = \mathbf{Z}(\Theta_i(A), \Psi_i(B), \hat{z}_i, \hat{F}_i)$ is the estimated point cloud representing the position of the atoms in the i -th particle (see (2.7) in subsection 2.3). The functions $\Theta_i(\cdot)$ and $\Psi_i(\cdot)$ in the definition of $\Gamma_i(A, B)$ are given by (1.2). Then, the estimated cryo-EM images are obtained by applying the forward operator to the estimated volume densities, i.e.

$$\hat{Y}_i(A, B) = \mathcal{F}[\hat{U}_i(A, B)] \in \mathbb{R}^{N \times N}, \quad \text{for } i \in \{1, \dots, n\}.$$

We can now formulate the following least squares problem to estimate the parameters $A = [\mathbf{a}_0, \mathbf{a}_1, \dots, \mathbf{a}_{K-1}]$ and $B = [\mathbf{b}_0, \mathbf{b}_1, \dots, \mathbf{b}_{K-1}]$ in (1.2) as

$$[\hat{A}, \hat{B}] := \underset{A, B}{\operatorname{argmin}} \frac{1}{n} \sum_{i=1}^n \|\hat{Y}_i(A, B) - Y_i\|^2,$$

where $\{Y_i\}_{i=1}^n$ are the 2D images in the cryo-EM dataset.

This is a non-convex minimization problem, and we may use stochastic gradient descent (SGD) to approximate a solution. As it is usual when applying iterative methods to approximate the solution of a non-convex problem, the success of the method heavily depends on the initialization of the parameters, in this case the vectors \mathbf{a}_k and \mathbf{b}_k in (1.2). Here is where the known conformation of the macromolecule, represented by the parameters (Θ_0, Ψ_0) , becomes very important. Indeed, for the initialization of the iterative method, we simply set all the parameters \mathbf{a}_k and \mathbf{b}_k to be equal to 0, so that the prediction of the atomic model for all the particles at the initialization is the known conformation. This provides a reasonable initial guess for the atomic model of each particle, which is then deformed, changing the conformation of the macromolecule, in order to improve the predictions to better fit the cryo-EM dataset.

In section 3 we provide some numerical experiments in which we use our method to reconstruct the heterogeneous atomic model of two flexible structures from noisy tomographic projections and a known conformation. In the first experiment (subsection 3.1), we consider a two-dimensional structure in which the discrete curve forms a flexible box with two moving arms. In this case, the density functions associated to the atomic structure are two-dimensional images, and the associated tomographic projections are therefore one-dimensional functions (see figure 6). In the second experiment (subsection 3.2), we consider a three-dimensional structure consisting of a protein backbone, which is continuously deformed following a trajectory simulated in [4] based on molecular dynamics (see figure 11). The discrete curve in this case represents the positions of the C- α atoms in the protein backbone.

The rest of the paper is structured as follows:

²In the original cryo-EM problem, the orientation of the particles is not available in general, however, since we are interested here on recovering the structural heterogeneity, we may assume that the orientations have been accurately estimated, previously, by means of existent methods as for instance RELION [25]

- (i) In section 2 we describe our method in detail. First, we introduce in subsection 2.1 the spectral decomposition of atomic structures satisfying the aforementioned discrete curve property. In subsection 2.2, we describe the method, based on manifold learning, to approximate the spectral decomposition by means of the cryo-EM dataset. In subsection 2.3, we formulate the minimisation problem which is used to estimate the coefficients in the spectral decomposition.
- (ii) In section 3 we present some numerical experiments in which we use our method to carry out the tomographic reconstruction of two-dimensional and three-dimensional atomic structures.
- (iii) At the end, we include Appendix A, where we describe the parametrisation of discrete curves, based on a discrete version of the Frenet frames [10], that we use throughout the paper; and Appendix B, where we describe the methods, taken from [2] and [17], to construct a low-dimension representation of the particles from the cryo-EM dataset, which is then used to build the graph Laplacian that we use in our method.

2. THE METHOD

In this section we describe our method in detail. See figure 3 for a high-level description of the method. We start by introducing the spectral decomposition of the atomic structure (subsection 2.1). Then, we describe the method that to approximate this spectral decomposition (subsection 2.2). Finally, we formulate the minimization problem that we use to estimate the coefficients in the spectral decomposition (subsection 2.3).

2.1. Spectral decomposition of the atomic structure. As mentioned in the introduction, our approach relies on the fact that we have prior knowledge about the molecular structure. This knowledge consists on knowing the number of atoms, the overall structure (whether it is a chain, a tree...), and having access to the 3D structure of the macromolecule in some specific conformation (this one can be obtained by using for instance AlphaFold [11]). These assumptions will be crucial later on to parametrize the set of possible molecular structures and carry out the spectral decomposition in the parameter space. In particular, we make the following structural assumption:

Assumption 1. *The molecular structure has a fixed number of $m \in \mathbb{N}$ atoms forming a chain (or discrete curve), i.e. there exists $\delta > 0$ such that the point cloud $\{z_1, z_2, \dots, z_m\} \in \mathbb{R}^{3m}$ representing the positions of the atoms satisfies*

$$\|z_{j+1} - z_j\| \approx \delta, \quad \forall j \in \{1, \dots, m-1\}.$$

Moreover, we assume that the set of conformations of the macromolecule, that will be denoted by \mathcal{M} , is a connected compact manifold of dimension $d \geq 1$, that can be embedded in a higher dimensional Euclidean space \mathbb{R}^q , with $q \geq d$.

Under this assumption, and considering that we know the number of atoms $m \in \mathbb{N}$ and the distance $\delta > 0$ between adjacent atoms, we will see in the appendix A that the atomic model associated to any conformation can be represented as the solution of a dynamical system of the

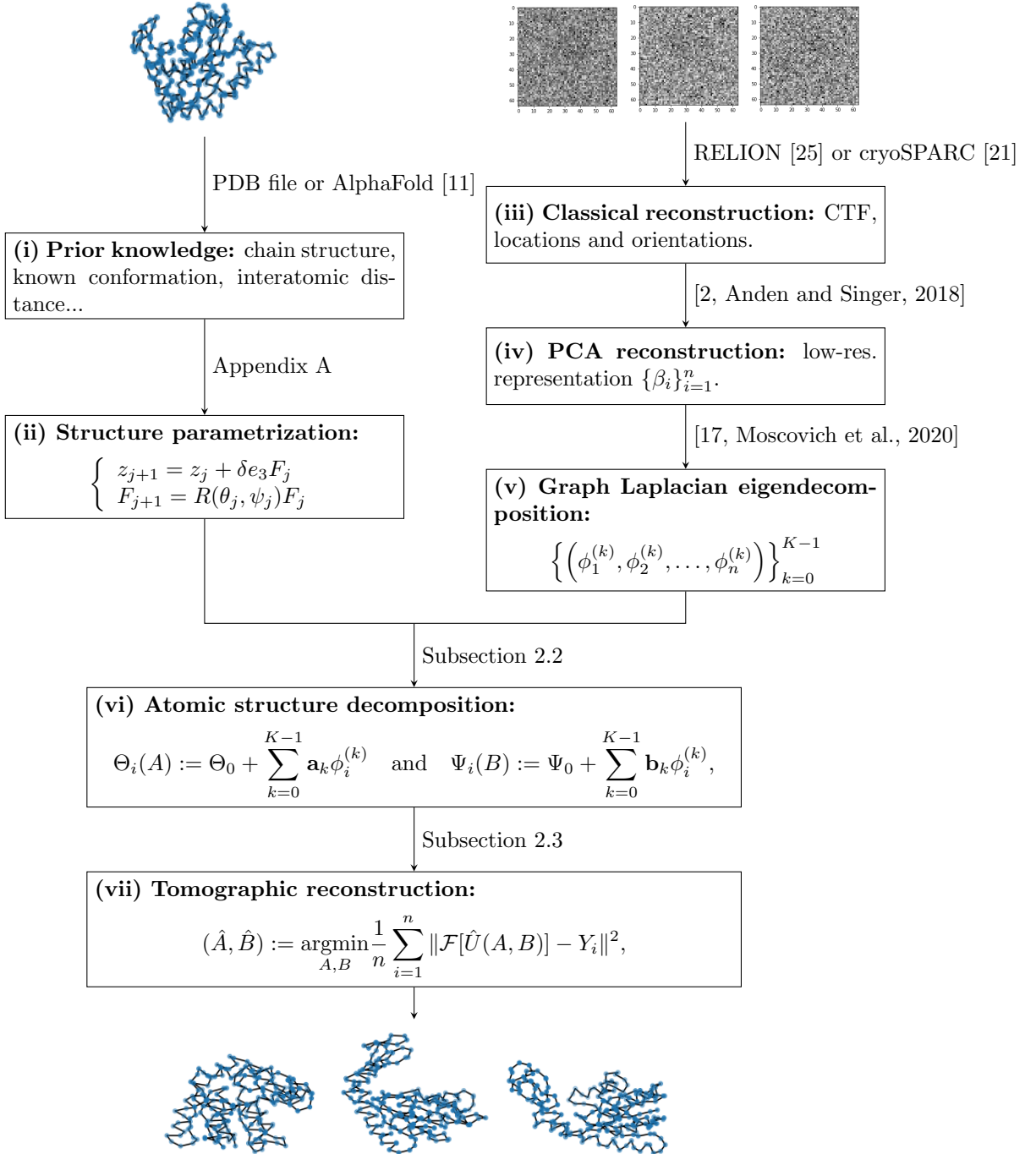


FIGURE 3. Diagram of our method. We observe that it combines prior biological knowledge about the macromolecule (in the left column) and the experimental data from cryo-EM (in the right column). The atomic structure decomposition in (vi) is constructed using the prior knowledge, whereas the coefficients are estimated by solving the minimization problem in (vii), using the cryo-EM images $\{Y_i\}_{i=1}^n$.

form

$$(2.1) \quad \begin{cases} z_{j+1} = z_j + \delta e_3 F_j & j \in \{1, \dots, m-1\} \\ F_{j+1} = R(\theta_j, \psi_j) F_j & j \in \{1, \dots, m-2\} \\ \text{with } z_{j_0} = \hat{z} \in \mathbb{R}^3 \text{ and } F_{j_0} = \hat{F} \in SO(3). \end{cases}$$

where $e_3 = (0, 0, 1) \in \mathbb{R}^3$, the sequence $\{z_1, \dots, z_m\} \subset \mathbb{R}^{3m}$ denotes the positions of the atoms in the macromolecule, and $\{F_1, \dots, F_{m-1}\} \subset SO(3)^{m-1}$ are the so-called Discrete Frenet Frames (see the appendix A and also [10] for further details). The inter-atomic distance $\delta > 0$ is fixed and given, $R(\theta_j, \psi_j) \in SO(3)$ denotes the rotation matrix in \mathbb{R}^3 with angles θ_j and ψ_j , i.e.

$$R(\theta_j, \psi_j) = \begin{pmatrix} \cos \psi_j \cos \theta_j & \cos \psi_j \sin \theta_j & -\sin \psi_j \\ -\sin \theta_j & \cos \theta_j & 0 \\ \sin \psi_j \cos \theta_j & \sin \psi_j \sin \theta_j & \cos \psi_j \end{pmatrix},$$

and the index $j_0 \in \{1, \dots, m-1\}$ in (2.1) is chosen a priori (typically in the middle of the chain). We observe that the space of such structures can be parametrized by the rotation angles (θ_j, ψ_j) at each point of the discrete curve, along with the initial condition (\hat{z}, \hat{F}) , which determines the spatial position and the orientation of the particle. Let us define the parameter space of such discrete curves as

$$(2.2) \quad (\Theta, \Psi, \hat{z}, \hat{F}) \in \mathcal{A} \times \mathcal{I} := ([-\pi, \pi]^{m-2} \times [-\pi, \pi]^{m-2}) \times (\mathbb{R}^3 \times SO(3)),$$

where $\Theta = (\theta_1, \dots, \theta_{m-2})$ and $\Psi = (\psi_1, \dots, \psi_{m-2})$ represent the torsion and bond angles at each point in the curve, and \hat{z} and \hat{F} determine the position and the orientation of the structure at the reference atom j_0 , that is chosen a priori, typically in the central part of the molecular structure. See more details about the parametrization of the atomic model in the appendix A.

The choice of the reference atom is arbitrary, but it is convenient to choose a point in a part of the structure which is invariant in all the conformations, i.e. we want z_{j_0} and F_{j_0} to depend only on the location and the orientation of the particle but not on the conformation. Choosing as reference an atom in a flexible part of the macromolecule would imply that the parameters \hat{z} and \hat{F} are also a function of the conformation, and therefore, these parameters should also be included in the spectral decomposition (1.2).

In the parametrization (2.1)-(2.2) of the atomic model we observe, on one hand, that the parameters \hat{z} and \hat{F} only determine the spatial location and the orientation of the particle. On the other hand, Θ and Ψ , which are invariant under rotations and translations of the particle, determine the three-dimensional structure up to rotations and translations. Roughly speaking, they determine the shape of the curve. The parameters Θ and Ψ are therefore the relevant parameters to describe the structural heterogeneity of the macromolecule, as modifying these parameters translates into deformations of the shape of the curve. Moreover, we stress that these deformations are translation and rotation invariant. In our numerical experiments in section 3, we shall assume the knowledge of the location and the orientation of the particles in the cryo-EM dataset, represented by the knowledge of \hat{z} and \hat{F} for each of the particles, so that the tomographic reconstruction reduces to estimate the parameters Θ and Ψ for each particle.

Denoting by \mathcal{M} the set of possible conformations, our goal is to construct a map

$$(2.3) \quad \eta \in \mathcal{M} \mapsto [\Theta(\eta), \Psi(\eta)] \in \mathcal{A} := [-\pi, \pi]^{m-2} \times [-\pi, \pi]^{m-2},$$

which maps any element in \mathcal{M} to the associated parameters Θ and Ψ , which determine a unique atomic model satisfying Assumption 1, up to rotations and translations. As mentioned in the introduction, a key reason of the success of our method relies on having access to the atomic model of the macromolecule in some specific conformation. This conformation will be used to initialise the iterative algorithm for the tomographic reconstruction of the 3D structure of each particle.

Assumption 2. *We consider that we know the atomic model of a single conformation of the macromolecule, and therefore, we can extract the number of atoms $m \in \mathbb{N}$ in the chain, the distance between adjacent atoms $\delta > 0$, and compute the torsion and bond angles denoted by $(\Theta_0, \Psi_0) \in \mathcal{A}$.*

As indicated in the introduction, we are interested in estimating the difference between the known atomic model and the atomic model associated to each conformation, i.e., $\Theta(\eta) - \Theta_0$ and $\Psi(\eta) - \Psi_0$ for every $\eta \in \mathcal{M}$. Following a similar idea as in [17], we construct the functions $\Theta(\cdot)$ and $\Psi(\cdot)$ as the linear combination of a finite number of elements in a basis of $L^2(\mathcal{M})$ as follows:

$$(2.4) \quad \Theta(\eta) = \Theta_0 + \sum_{k=0}^{K-1} \mathbf{a}_k \phi_k(\eta) \quad \text{and} \quad \Psi(\eta) = \Psi_0 + \sum_{k=0}^{K-1} \mathbf{b}_k \phi_k(\eta),$$

where $K \in \mathbb{N}$ is chosen a priori, $\phi_k(\cdot) : \mathcal{M} \rightarrow \mathbb{R}$, for $k \in \{0, 1, \dots, K-1\}$ are the eigenfunctions associated to the K smallest eigenvalues of the Laplace-Beltrami operator in \mathcal{M} , and $\mathbf{a}_k \in \mathbb{R}^{m-2}$ and $\mathbf{b}_k \in \mathbb{R}^{m-2}$ for $k \in \{0, 1, \dots, K-1\}$ are the coefficients of the spectral decomposition of the atomic structure.

Remark 2.1. *We see in (2.4) that we are actually estimating the deformation of the molecular structure with respect to the given known conformation. As we will see in the sequel, this assumption about the known conformation is extremely important in the estimation of the coefficients \mathbf{a}_k and \mathbf{b}_k in (2.4). Indeed, the estimation of \mathbf{a}_k and \mathbf{b}_k is addressed by means of SGD applied to a non-convex minimisation problem. As initialisation we take all the coefficients \mathbf{a}_k and \mathbf{b}_k to be equal to 0, so that the initial guess of the atomic model for any particle coincides with the known conformation. This produces reasonable predictions for all the particles that, by applying SGD, are then deformed to fit the cryo-EM data and obtain the atomic model approximating the conformation of each particle.*

Remark 2.2. *We recall, from Assumption 1, that \mathcal{M} is a connected compact manifold, and hence, the eigenfunctions of the Laplace-Beltrami operator in \mathcal{M} form a complete orthonormal basis of $L^2(\mathcal{M})$. Moreover, it is well-known [5, 9] that the eigenvalues $0 = \lambda_0 < \lambda_1 \leq \lambda_2 \leq \dots$ give an estimate of the regularity of the associated eigenfunctions $\{\phi_0(\cdot), \phi_1(\cdot), \phi_2(\cdot), \dots\}$. This can be interpreted as follows: in the expansion of any smooth function in \mathcal{M} as a linear combination of the eigenfunctions, the terms associated to higher eigenvalues correspond to higher frequencies of the function. By using only the eigenfunctions associated to the smaller eigenvalues in the spectral decomposition (2.4), we only capture deformations of the molecular structure of low frequency in \mathcal{M} . We note that in this work, we aim at describing only the large deformations of the macromolecule, and we are not interested in high-frequency deformations, which are typically associated to small vibrations of the atoms.*

Remark 2.3. *Another interesting feature of our approach is the fact that we can use prior knowledge about the macromolecule to reduce the number of coefficients to be estimated in (1.2). Some parts of the macromolecules may be known to be very stable, so that their internal structure is preserved in all the conformations. This is the case, for instance, of the so-called secondary structures*

appearing in proteins (α -helices and β -strands). These substructures only suffer rigid transformations (rotations and translations) from one conformation to another, and then the functions $\theta_i(\eta)$ and $\psi_i(\eta)$ associated to the atoms conforming these substructures should be constant in \mathcal{M} . This can be achieved by using only the first term in the expansion (1.2) (i.e. we set the parameters $a_{k,i} = 0$ and $b_{k,i} = 0$ for all $k \geq 1$), since we know that the first eigenfunction $\phi_0(\cdot)$ is constant in \mathcal{M} . An intermediate situation can be also considered, in which one may use a different number of eigenfunctions in the expansion (1.2) (by setting the corresponding coefficients to zero), depending on the prior knowledge about the flexibility of certain parts of the molecular structure. See the numerical experiments in subsections 3.1.1 and 3.1.2 for an illustration of the feature described in this remark.

2.2. Approximated spectral decomposition. In single particle cryo-EM, we have access to a dataset with noisy tomographic projections of a macromolecule in different conformations, and taken from different viewing directions. This is the data that we want to use in order to determine the atomic model of the macromolecule in all its conformations by approximating the spectral decomposition introduced in subsection 2.1. As outlined above, under Assumption 1, the problem consists on estimating the map $[\Theta(\cdot), \Psi(\cdot)]$ defined in (2.3). In our approach, the functions $\Theta(\cdot)$ and $\Psi(\cdot)$ are estimated by means of an expansion series of the form (2.4). We see that one needs two ingredients: the eigenfunctions of the Laplace-Beltrami operator in \mathcal{M} , and the vector coefficients $\mathbf{a}_k \in \mathbb{R}^{m-2}$ and $\mathbf{b}_k \in \mathbb{R}^{m-2}$, where m is the number of atoms in the chain. The estimation of the latter will be addressed in the following subsection. For the former, we have the difficulty of not knowing the manifold \mathcal{M} , however, we can apply the same strategy as in [17], based on manifold learning, to obtain a spectral approximation of \mathcal{M} by means of a suitable graph Laplacian, constructed from the cryo-EM dataset. This method builds on the assumption that we have a low-dimension representation of the conformation of each particle in the dataset.

Assumption 3. For each image in the cryo-EM dataset $\{Y_i\}_{i=1}^n$ we have a low-dimension representation $\{\beta_i\}_{i=1}^n \subset \mathbb{R}^q$ of the conformation of the particle in each image, so that the manifold of conformations \mathcal{M} can be embedded in \mathbb{R}^q . Moreover, this representation is independent of the viewing direction of the tomographic projection, so that $\{\beta_i\}_{i=1}^n$ can be seen as a discrete approximation of the manifold \mathcal{M} .

In [17], the low-dimension representation of the heterogeneity consists on the PCA coefficients of the low-resolution reconstruction of the particles obtained by the method in [2]. For the independence of β_i with respect to the viewing direction, this assumption can be justified by assuming that the reconstruction from [2] is accurate independently of the orientation of the particle. Now, using this low-dimension representation of the dataset, we construct a weighted graph with the similarities between the conformations in every two particles, and compute the eigenvectors associated to the smallest eigenvalues of the symmetric normalized Laplacian matrix associated to the graph of similarities (see more details in the appendix B).

Let $K \in \mathbb{N}$ be fixed, let $L \in \mathcal{S}(n)$ be the symmetric graph Laplacian matrix associated to the aforementioned matrix of similarities, and let

$$(2.5) \quad \Phi = [\phi^{(0)} | \phi^{(1)} | \dots | \phi^{(K-1)}] \in \mathbb{R}^{n \times K}$$

be the matrix which has, as columns, the eigenvectors $\phi^{(k)} \in \mathbb{R}^n$ associated to the K smallest eigenvalues of the graph Laplacian matrix L . Some definitions of the graph Laplacian are known

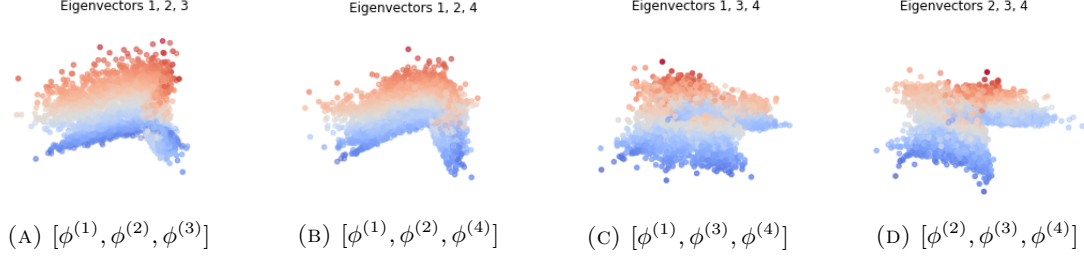


FIGURE 4. Representation of the eigenvectors $\phi^k \in \mathbb{R}^n$ of the graph Laplacian constructed from the synthetic dataset of two-dimensional structures presented in subsection 3.1. Each plot can be seen as an approximation of the manifold of conformations \mathcal{M} projected in different three-dimensional linear spaces.

to converge to a continuous operator in \mathcal{M} , in the sense that the eigenvectors $\phi^{(k)}$ of the graph Laplacian converge to the eigenfunctions $\phi_k(\cdot)$ of this operator [13, 22, 29]. In some cases, the limit operator is the Laplace-Beltrami operator in \mathcal{M} , but actually, we only need that the eigenfunctions of the limit operator form an orthonormal basis of $L^2(\mathcal{M})$.

As in [17, Section 5.3], we assume that the ordered eigenvectors $\phi^{(0)}, \phi^{(1)}, \dots \in \mathbb{R}^n$ of the graph Laplacian converge in probability to a set of eigenfunctions $\phi_0(\cdot), \phi_1(\cdot), \dots : \mathcal{M} \rightarrow \mathbb{R}$ of some continuous linear differential operator on \mathcal{M} , in the sense that, for all $k \in \mathbb{N}$, we have

$$\sup_{i=1, \dots, n} |\sqrt{n} \phi_i^{(k)} - \phi_k(\beta_i)| \rightarrow 0 \quad \text{as } n \rightarrow \infty.$$

Furthermore, we assume that this set of eigenfunctions $\{\phi_k(\cdot)\}_{k=0}^\infty$ form an orthonormal basis of $L^2(\mathcal{M})$. Hence, for each particle u_i in the cryo-EM dataset, we can estimate the parameters $[\Theta_i, \Psi_i]$ of the corresponding conformation by approximating the expression (2.4) as

$$(2.6) \quad \Theta_i(A) = \Theta_0 + \sum_{k=0}^{K-1} \mathbf{a}_k \phi_i^{(k)} = \Theta_0 + A \Phi_i \quad \text{and} \quad \Psi_i(B) = \Psi_0 + \sum_{k=0}^{K-1} \mathbf{b}_k \phi_i^{(k)} = \Psi_0 + B \Phi_i$$

where $A = [\mathbf{a}_0, \mathbf{a}_1, \dots, \mathbf{a}_{K-1}] \in \mathbb{R}^{(m-2) \times K}$ and $B = [\mathbf{b}_0, \mathbf{b}_1, \dots, \mathbf{b}_{K-1}] \in \mathbb{R}^{(m-2) \times K}$ are the matrices of coefficients, and $\Phi_i \in \mathbb{R}^K$, for $i = 1, \dots, n$, are the column vectors with the i -th component of each eigenvector from (2.5), i.e.

$$\Phi_i = (\phi_i^{(0)}, \phi_i^{(1)}, \dots, \phi_i^{(K-1)}) \in \mathbb{R}^K.$$

2.3. Tomographic reconstruction. We here formulate the minimization problem that we use to estimate the coefficients A and B in the spectral decomposition (2.6). As mentioned in the introduction, in this work we are interested in recovering the structural heterogeneity of the macromolecule, and therefore we assume that the position and the orientation of the particles have been already estimated, for instance, by using existent methods such as RELION [25].

Assumption 4. For each 2D image in the cryo-EM dataset $\{Y_i\}_{i=1}^n$, we know the 3D orientation and the position of the underlying particle, i.e. we know the parameters \hat{z}_i and \hat{F}_i associated to each particle u_i .

Using the expression (2.6) for the rotation angles, along with the known 3D spatial location $\hat{z}_i \in \mathbb{R}^3$ and orientation $\hat{F}_i \in SO(3)$ of each particle, we can estimate the positions of the atoms in the molecular structure as the solution to the dynamical system (2.1). For every particle $i \in \{1, \dots, n\}$, we denote the associated point cloud by

$$(2.7) \quad \Gamma_i(A, B) := \mathbf{Z}(\Theta_i(A), \Psi_i(B), \hat{z}_i, \hat{F}_i) = [z_1, z_2, \dots, z_m] \in \mathbb{R}^{3m},$$

where $\mathbf{Z} : \mathcal{A} \times \mathcal{I} \rightarrow \mathbb{R}^{3m}$ is the operator which associates, to each set of parameters $(\Theta, \Psi, \hat{z}, \hat{F}) \in \mathcal{A} \times \mathcal{I}$, the solution to the dynamical system (2.1). See appendix A for more details.

Then, the 3D electrostatic potential of the underlying particle is estimated as a sum of Gaussian densities centred at the atom positions, i.e.

$$(2.8) \quad \hat{U}_i(A, B)(x) = \sum_{z_j \in \Gamma_i(A, B)} \nu \exp \left[-\frac{\|x - z_j\|^2}{2\sigma^2} \right], \quad \forall x \in \mathbb{R}^3,$$

where $\nu, \sigma > 0$ are hyperparameters which can be typically known from the chemical composition of the macromolecule.

Finally, in order to compare the reconstructions with the cryo-EM images, we apply the forward cryo-EM operator \mathcal{F} to the potential $\hat{U}_i(A, B)(\cdot)$ estimated for each particle, and evaluate it in the 2D grid formed by the pixel positions of the images. Let $\mathbf{X} := \{x_{\alpha, \beta}\}_{\alpha, \beta=(1,1)}^{(N,N)} \in (\mathbb{R}^2)^{N \times N}$ be the rectangular grid corresponding to the pixel positions of the cryo-EM images. Then we define $\hat{Y}_i(A, B) = \{\hat{y}_{\alpha, \beta}^{(i)}\}_{\alpha, \beta=(1,1)}^{(N,N)}$ as

$$(2.9) \quad \hat{y}_{\alpha, \beta}^{(i)}(A, B) = \mathcal{F}[\hat{U}_i(A, B)](x_{\alpha, \beta}) \quad \text{for all } (\alpha, \beta) \in \{1, 2, \dots, N\}^{N \times N},$$

where the forward operator \mathcal{F} is the tomographic projection along the vertical axis, followed by a 2D convolution with the point spread function, that is assumed to be known.

The parameters A and B in (2.6) are estimated by means of a minimisation problem, in which the loss functional is the mean square error between the clean cryo-EM images \hat{Y}_i given by the estimated atomic model and the noisy cryo-EM images Y_i from the dataset, i.e.

$$(2.10) \quad [\hat{A}, \hat{B}] = \underset{A, B}{\operatorname{argmin}} \frac{1}{n} \sum_{i=1}^n \|\hat{Y}_i(A, B) - Y_i\|_2^2.$$

Remark 2.4. *A solution to the minimisation problem (2.10) can be approximated by SGD algorithm. The main difficulty comes from the fact that the function $\hat{Y}_i(A, B)$ is non-linear with respect to A and B , and therefore, the loss functional to be minimised is not necessarily convex. Moreover, the parameter space $(A, B) \in [\mathbb{R}^{(m-2) \times K}]^2$ has a rather high dimension. In this high-dimensional non-convex situations, the success of iterative algorithms such as SGD heavily depends on having a good initialisation of the parameters. Here is where Assumption 2 becomes very important. Indeed, having the rotation angles (Θ_0, Ψ_0) of a known conformation allows us to initialize the algorithm in such a way that the predicted structure for all the particles is the given known conformation. In view of (2.6), this can be achieved simply by initializing A and B to be equal to 0 in all of their components. This gives a reasonable initial guess for all the particles, which are then deformed, by modifying A and B , in order to better fit the cryo-EM dataset.*

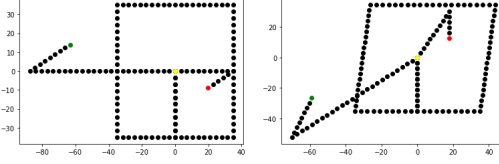


FIGURE 5. Two-dimensional structure in the given conformation (at the left) and a different conformation (at the right). The first point z_1 is coloured in green, the end point z_m in red, and the reference point z_{j_0} in yellow. Note that the curve self-intersects along the segment joining the box and the arms.

3. NUMERICAL EXPERIMENTS

In this section, we present some numerical experiments in which we apply our method to carry out the tomographic reconstruction of flexible atomic structures in two synthetic datasets. In the first dataset, the underlying structure is a two-dimensional discrete curve, which forms a flexible box and two moving arms (see figure 5). The volumetric representations of the structure are therefore functions in \mathbb{R}^2 , and the associated tomographic projections are one-dimensional functions (see figure 6). Although in the above, we have presented our method in a three-dimensional setting, it is not difficult to adapt all the steps in our method to a two-dimensional structure with one-dimensional tomographic projections. In the second dataset, the underlying structure is a protein backbone, composed by the C- α atoms, which is deformed following a simulated molecular trajectory from [4] using molecular dynamics (see Figure 11). In this case the structure is three-dimensional, and we can therefore apply our method exactly as it is presented in the above.

3.1. Two-dimensional structure. In this experiment, we consider a two-dimensional structure consisting of a discrete curve with $m = 149$ points and inter-atomic distance $\delta = 3.5$. The atomic structure can be represented using the same construction as in Appendix A, adapted to a two-dimensional setting:

$$(3.1) \quad \begin{cases} z_{j+1} = z_j + \delta e_2 F_j & j \in \{1, \dots, m-1\} \\ F_{j+1} = R(\theta_j) F_j & j \in \{1, \dots, m-2\} \\ \text{with } z_{j_0} = \hat{z} \in \mathbb{R}^2 \text{ and } F_{j_0} = \hat{F} \in SO(2). \end{cases}$$

where $e_2 = (0, 1) \in \mathbb{R}^2$, $\{z_j\}_{j=1}^m \in \mathbb{R}^{2m}$ denote the positions of the atoms and $\{F_j\}_{j=1}^{m-1} \in SO(2)^{m-1}$ denote the discrete Frenet frames at each point in the curve. Note that, since we have a two-dimensional structure, the rotation matrices $R(\theta_j) \in SO(2)$ are parametrized by a single angle and are given by

$$R(\theta_j) := \begin{bmatrix} \cos \theta_j & -\sin \theta_j \\ \sin \theta_j & \cos \theta_j \end{bmatrix}.$$

In the synthetic dataset that we have generated, the two-dimensional structure is a discrete curve forming a flexible box with two moving arms (see Figure 5). The arms and the box are joined by a segment, along which the atomic structure self-intersects. We see that all the rotation angles θ_j are equal to 0 except for the points in the corners of the structure. In this experiment, the angles

determining the position of the arms are given by

$$(3.2) \quad \theta_{33} = -\frac{\pi}{2} + \tilde{\theta}_{33} \quad \text{and} \quad \theta_{133} = -\frac{\pi}{2} + \tilde{\theta}_{133},$$

where $\tilde{\theta}_{33}$ and $\tilde{\theta}_{133}$ are random variables uniformly distributed in $[-\pi/2, \pi/2]$, and the angles determining the form of the box are given by

$$(3.3) \quad \theta_{53} = \theta_{93} = -\frac{\pi}{2} + \tilde{\theta}_{box} \quad \text{and} \quad \theta_{73} = \theta_{123} = -\frac{\pi}{2} - \tilde{\theta}_{box}$$

where $\tilde{\theta}_{box}$ is a random variable uniformly distributed in $[-\pi/4, \pi/4]$. As reference point we have chosen $j_0 = 33$, which is in a part of the structure invariant in all the conformations (see Figure 5).

In this two-dimensional case, the electrostatic potential associated to each particle is not a volumetric density, but rather a two-dimensional image. For the given point cloud $\{z_j\}_{j=1}^m \in \mathbb{R}^{2m}$ we define the associated two-dimensional image as

$$(3.4) \quad u(x) = \sum_{j=1}^m \exp \left[-\frac{\|x - z_j\|^2}{2\sigma^2} \right], \quad \forall x \in \mathbb{R}^2,$$

with $\sigma = 7$. In our numerical experiments we have considered no point spread function. The forward operator is modelled as the tomographic projection of the function $u(x)$ along the vertical axis, resulting in a one-dimensional function.

In order to generate the synthetic cryo-EM dataset, we have generated 4000 structures as defined above, where the point cloud is given by (3.1), with the rotation angles given by (3.2)–(3.3). Then, each structure is rotated by choosing \hat{F} uniformly at random in $SO(2)$. With the 4000 structures, we have generated the associated two-dimensional images $\{u_i\}_{i=1}^{4000}$ as in (3.4). Then, we have computed the one-dimensional tomographic projections by integrating the two-dimensional images along the vertical axis, i.e.

$$Y_i = T(u_i) + \xi_i, \quad \text{for } i = 1, \dots, 4000,$$

where $T(\cdot)$ denotes the tomographic projection of u_i along the vertical axis, evaluated on a one-dimensional grid with 128 discretisation points. We have also added Gaussian noise $\xi_i \in \mathbb{R}^{128}$, where each component follows a Gaussian distribution with variance 2500. The variance of the clean images is 182.63, so the signal to noise ratio of the dataset is

$$SNR = \frac{182.63}{2500} = 0.073.$$

As mentioned in Assumption 3, we assume that we have a low-dimension reconstruction of the particles in the cryo-EM dataset (this one can be obtained by the method in [2]). In our case, this low-dimension representation of the particles comes in the form of noisy two-dimensional images of size 64×64 , that we call $\{U_i\}_{i=1}^{4000} \subset \mathbb{R}^{64 \times 64}$. Each image U_i is defined as the function (3.4) associated to the i -th point cloud, evaluated in a 2D grid. We then added Gaussian noise with variance 9 to each low-resolution image. With this images we have constructed the weighted graph of similarities, using a Gaussian kernel of the form

$$(3.5) \quad W_{ij} = \exp \left[-\frac{\|U_i - U_j\|^2}{2\sigma^2} \right], \quad \text{with } \sigma = 96.$$

Then we have constructed the normalized graph Laplacian and computed the eigenvectors associated to the 20 smallest eigenvalues. In Figure 4 we see the representation of some of these eigenvectors.

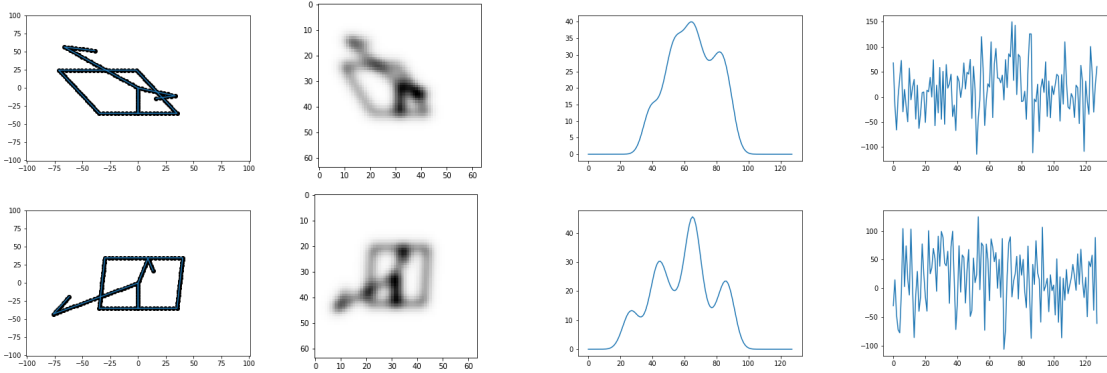


FIGURE 6. From left to right: the two-dimensional structure, the two-dimensional density function, the clean tomographic projection and the noisy tomographic projection.

These plots can be seen as an approximation of the manifold of conformations \mathcal{M} . Note that this structure has three degrees of freedom (the movement of the two arms plus the deformation of the box), and therefore, the manifold of conformations is expected to have dimension 3.

The next step in our method is to construct the spectral decomposition of the rotation angles θ_j with $j = 1, \dots, m-2$. Note that in the two-dimensional case we only need to estimate one rotation angle θ_j at each point in the curve, as opposed to two angles in the case of three-dimensional structures. Let us denote the sequence of rotation angles for the i -th particle as

$$\Theta_i = [\theta_1, \theta_2, \dots, \theta_{m-2}] \in [-\pi, \pi]^{m-2}.$$

As aforementioned, we assume to have access to a conformation of the structure (see Assumption 2). In this case, the given conformation (see figure 5) is the structure with the arms horizontally aligned and the box forming a square, i.e. we take $\tilde{\theta}_{33} = \tilde{\theta}_{133} = \tilde{\theta}_{box} = 0$ in (3.2) and (3.3). Following subsection 2.2, the parameter Θ_i for each particle is estimated as

$$\Theta_i = \Theta_0 + A\Phi_i,$$

where $\Phi_i \in \mathbb{R}^{20}$ is the vector with the i -th component of each of the first eigenvectors of the graph Laplacian computed before.

The last step in our method is to estimate the matrix $A \in \mathbb{R}^{(m-2) \times 20}$, which we address by following subsection 2.3. We will consider two cases for the tomographic reconstruction. In the first one, we use the knowledge of the angles that are actually varying, i.e. (3.2) and (3.3). Note that, by the construction of this particular structure, most of the rotation angles are equal to 0 in all the conformations. In the second case, we do not assume such knowledge about the angles which are actually varying, and therefore, the entire vector Θ_i is estimated. From a practical viewpoint a similar assumption may hold if one knows which parts in the macromolecule are flexible and which are not. For instance, it is known that the secondary structures in proteins, such as α -helices and β -strands are preserved from one conformation to another (see Remark 2.2).

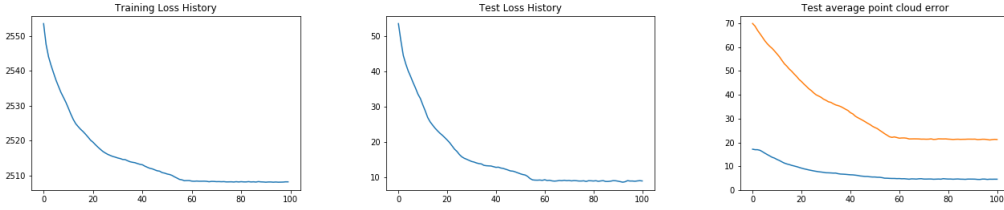


FIGURE 7. Evolution of the loss functional and the error in the predictions with respect to the ground truth for the 2D reconstructions, using the prior knowledge about the varying parameters (subsection 3.1.1).

The coefficients in the matrix A are estimated by applying SGD to the minimisation problem (2.10). In the minimisation problem, we use only 90 percent of the data ($n = 3600$ noisy tomographic projections). The rest of the data ($n = 400$ clean tomographic projections) are used to test the accuracy of the reconstructed structures. In both cases, we have applied 100 epochs of SGD algorithm with a batch size of 500. As for the learning rate, in the case in which only the varying parameters are estimated (subsection 3.1.1) we used a learning rate of 0.1, whereas in the case in which all the parameters are estimated (subsection 3.1.2) it seems to be necessary to take a smaller learning rate, and we have chosen 0.01 for this case. In both cases, we used the PyTorch implementation of the SGD algorithm, and it took around 2 minutes to compute 100 epochs of SGD in a MacBook Pro 1.4 GHz Intel Core i5 with 16 GB of RAM memory.

3.1.1. *Reconstruction estimating only the varying angles.* In this case, we assume that we know the angles that are actually varying in the structure, i.e. in view of (3.2) and (3.3), we only need to estimate the components $\theta_{33}, \theta_{53}, \theta_{73}, \theta_{93}, \theta_{123}$ and θ_{133} in each vector Θ_i . All the other parameters in Θ_i are given by the known conformation Θ_0 . In Figure 7, at the left, we observe the evolution of the loss function evaluated after every epoch of the SGD algorithm. In the centre we see the evolution of the loss function evaluated on the test data. Note that the test data consists of clean tomographic projections, and therefore, the loss is much smaller. At the right we see the evolution of the distance between the predicted point clouds for the test data $\{\tilde{z}_i\}_{i=1}^{400}$ and the ground truths $\{z_i\}_{i=1}^{400}$. The orange line in figure 7 represents the maximum over the point cloud

$$(3.6) \quad \frac{1}{400} \sum_{i=1}^{400} \max_{j=1, \dots, m} \|z_{i,j} - \tilde{z}_{i,j}\|,$$

whereas the blue line represents the total average error in the predicted point cloud with respect to the ground truth, i.e.

$$(3.7) \quad \frac{1}{400m} \sum_{i=1}^{400} \sum_{j=1}^m \|z_{i,j} - \tilde{z}_{i,j}\|.$$

In Figure 8 we see some of the reconstructions of the 2D structures. Of course, using the knowledge of which parameters are varying and which are invariant over the conformations yields significantly better reconstructions as compared to the reconstructions obtained in the following subsection 3.1.2, where such a knowledge is not assumed.

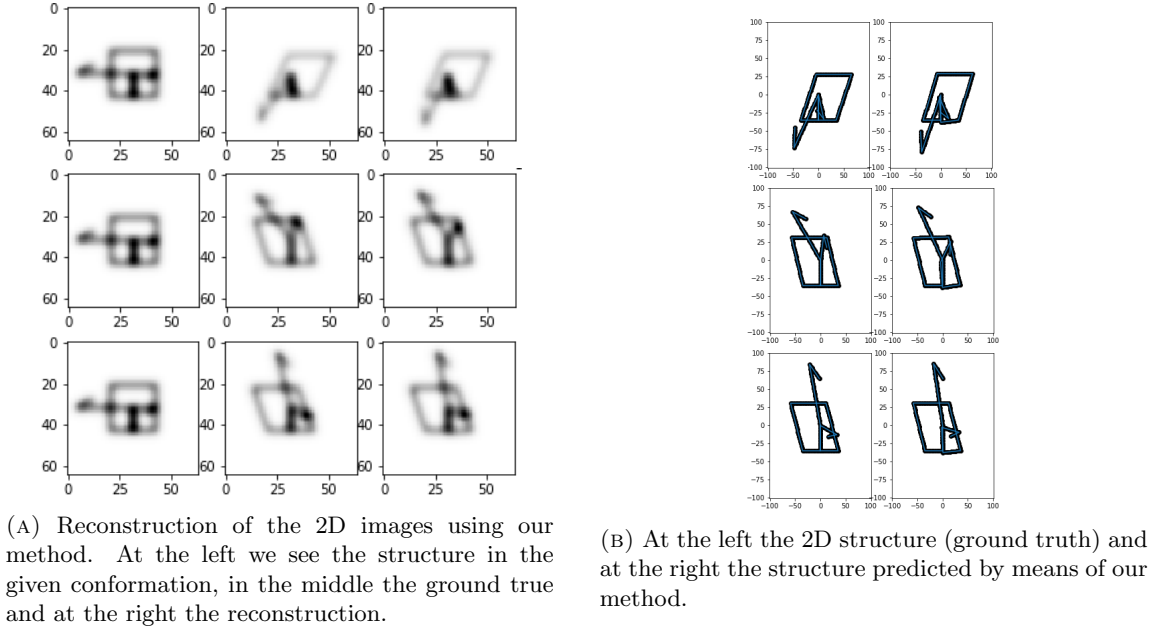


FIGURE 8. Some examples of the tomographic reconstruction of two-dimensional structures from tomographic projections. In this case we used the knowledge of the parameters that are varying.

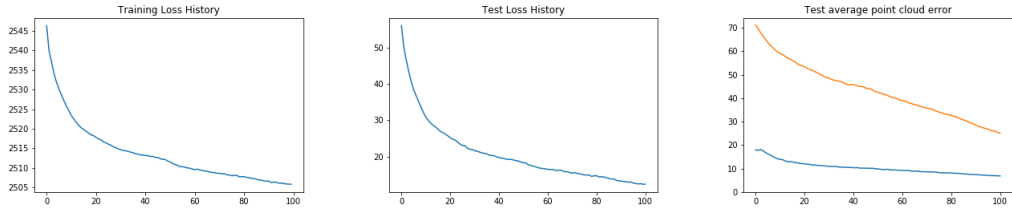


FIGURE 9. Evolution of the loss functional and the error in the predictions with respect to the ground truth for the 2D reconstructions, without using the prior knowledge about the varying parameters (subsection 3.1.2).

3.1.2. *Reconstruction estimating all the angles.* As opposite to the previous case, we now do not assume the knowledge of the varying parameters in the structure, and therefore we estimate the spectral decomposition of all the rotation angles in Θ . In Figure 9 we see the evolution of the loss functional over the epochs of the SGD algorithm as well as the error in the predicted point clouds in the test dataset (we recall that the orange line is given by (3.6) and the blue line is given by (3.7) in the previous subsection). We observe in Figure 10 that the predicted reconstructions are less accurate as compared with the reconstructions obtained when we know the parameters that are varying.

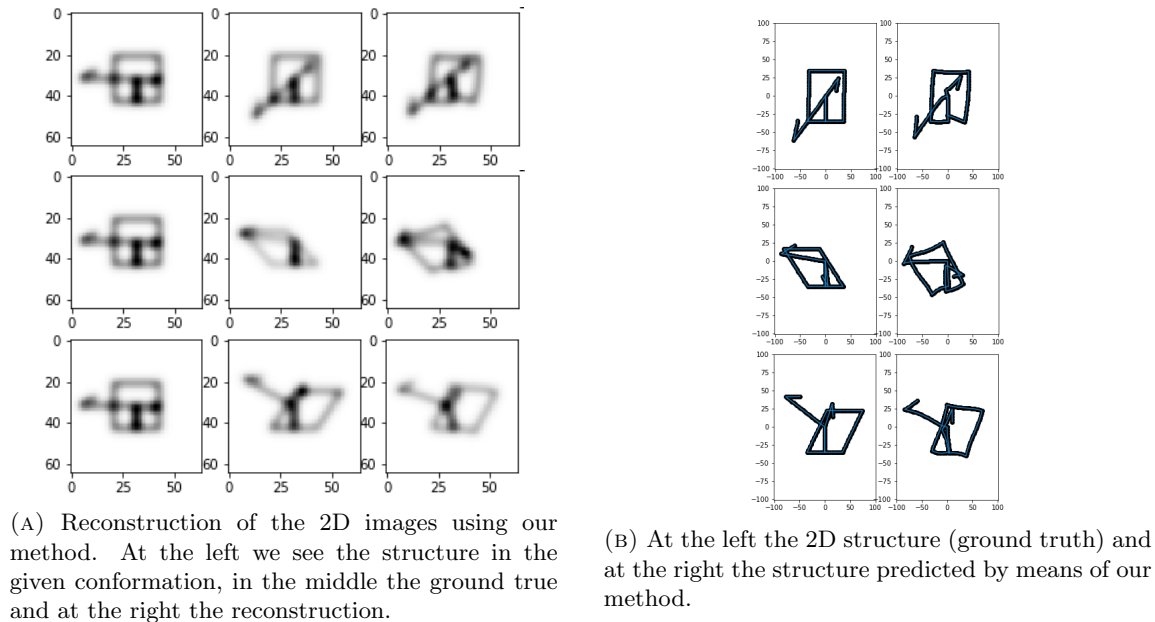


FIGURE 10. Some examples of the tomographic reconstruction of two-dimensional structures from tomographic projections. In this case we did not use the knowledge of the parameters that are varying, and therefore, all the parameters are estimated.

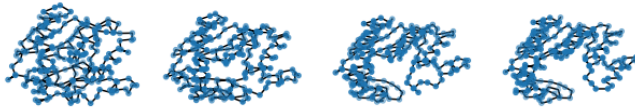


FIGURE 11. For frames of the backbone trajectory used in the numerical experiments in subsection 3.2.

3.2. Three-dimensional structure. In this experiment we consider a three-dimensional atomic structure satisfying the chain property from Assumption 1. The structure corresponds to the backbone of a protein with 214 amino-acid residues, from which we have extracted the positions of the $C-\alpha$ atoms. The motion of the protein structure is a simulation taken from [4] using molecular dynamics, and the result is a video with 102 frames in which the backbone is continuously deformed (see figure 11). In the whole trajectory, the distance between adjacent $C-\alpha$ atoms in the backbone is approximately constant, with average 3.8413 and variance 0.0067. In the reconstruction of the atomic structure, we have used a constant inter-atomic distance $\delta = 3.8412$. This choice produces small errors in the reconstructions as the inter-atomic distances in the dataset (ground truth) slightly vary due to small vibrations of the atoms. However, these errors do not seem to be very relevant in our reconstruction. As reference point in our reconstructions we have chosen the middle point in the discrete curve, i.e. the point $j_0 = 112$.

In order to generate a synthetic cryo-EM dataset, we have chosen 4000 structures randomly selected from the 102 frames of the backbone trajectory. Then, each particle is rotated by selecting a random rotation matrix $\hat{F}_i \in SO(3)$. The cryo-EM images $\{Y_i\}_{i=1}^{4000}$ are modelled as the noisy tomographic projection of the density volumes associated to each particle, with no point spread function. These volumes are represented by the sum of Gaussian functions centred at the C- α positions as in (2.8), i.e.

$$(3.8) \quad u(x) = \sum_{j=1}^{214} \exp \left[-\frac{\|x - z_j\|^2}{2\sigma^2} \right], \quad \forall x \in \mathbb{R}^3,$$

with $\sigma = 3$, and where $\{z_j\}_{j=1}^{214} \in \mathbb{R}^{3 \times 214}$ are the positions of the C- α atoms. The cryo-EM images are therefore given by

$$Y_i = T(u_i) + \xi_i, \quad \text{for } 1, \dots, 4000$$

where $T(\cdot)$ is the tomographic projection of the 3D density volume $u_i(\cdot)$, along the vertical axis, evaluated in a 64×64 two-dimensional grid. The additive noise $\xi_i, \in \mathbb{R}^{64 \times 64}$ is chosen to be Gaussian in each pixel with variance 1089. The variance of the clean images is of approximately 10, resulting in a cryo-EM dataset with signal to noise ratio

$$SNR = \frac{10}{1089} \approx 0.01.$$

See figure 1 for two samples in the synthetic cryo-EM dataset that we have used in this experiment.

Just as in the numerical experiment in subsection 3.1, we assume that we have a low-dimension representation of the 3D volumes associated to the particles, i.e. Assumption 3. In this case, these low-dimension representations are the density volumes (3.8) associated to each particle, evaluated in a 3D voxel grid of size $16 \times 16 \times 16$. With these low-dimension representation of the 3D volumes $\{U_i\}_{i=1}^{4000} \subset \mathbb{R}^{16 \times 16 \times 16}$, we construct a weighted graph with weights given by (3.5), in this case with $\sigma = 80$. Then, we have constructed the normalized graph Laplacian matrix associated to the above graph, and computed the eigenvectors associated to the 10 smallest eigenvalues. In this case, we have chosen only 10 eigenvectors because the dynamics of the structure seem to be simpler than in the two-dimensional example. Recall that in the two-dimensional experiment, the structure has three degrees of freedom, whereas here, we have a molecular trajectory, so the underlying manifold of conformations \mathcal{M} is expected to be one-dimensional (see figure 12 for a representation of some of the eigenvectors). In the molecular trajectory, we also observe high-frequency vibrations of the atoms, however, by keeping the number of eigenvectors rather small in the spectral decomposition, we are not recovering these vibrations (see Remark 2.2).

Following subsection 2.2, we construct the rotation angles for each particle as a linear combination of the 10 first eigenvectors, i.e.

$$\Theta_i = \Theta_0 + A\Phi_i \quad \text{and} \quad \Psi_i = \Psi_0 + B\Phi_i,$$

where Θ_0 and Ψ_0 are the rotation angles associated to the known conformation (see Assumption 2). In this experiment, we have chosen the known conformation (Θ_0, Ψ_0) to be the that of the particle in the first frame of the molecular trajectory (the atomic structure at the left in figure 11).

In the tomographic reconstruction we have not assumed any prior knowledge about the flexibility of the different parts of the atomic structure nor the secondary structures, and therefore, all the parameters in Θ and Ψ are estimated in the same way. The coefficients in the spectral decomposition

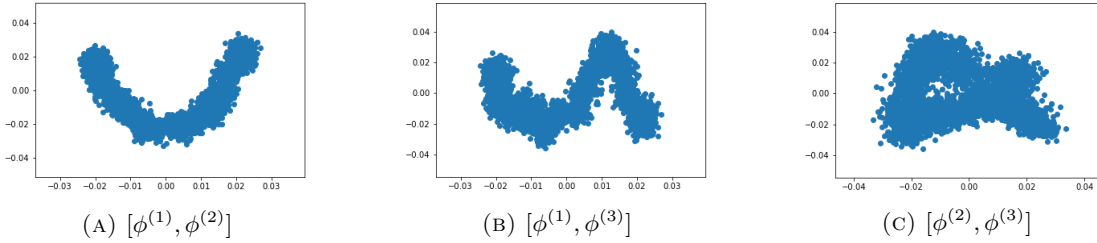


FIGURE 12. Representation of the eigenvectors $\phi^k \in \mathbb{R}^n$ of the graph Laplacian constructed from the synthetic dataset of three-dimensional structures. Each plot can be seen as an approximation of the manifold of conformations \mathcal{M} projected in different two-dimensional linear spaces.



FIGURE 13. Evolution of the loss functional and the error in the predictions with respect to the ground truth for the 3D reconstructions in subsection 3.2.

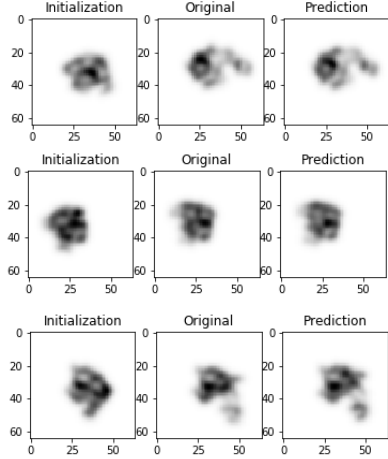
of the rotation angles Θ and Ψ are estimated by means of SGD applied to the minimisation problem (2.10) in subsection 2.3. As before, we have used only 90 percent of the cryo-EM data (3600 noisy tomographic projections) in the minimisation problem, leaving the remaining 10 percent (400 clean tomographic projections) to evaluate the quality of the reconstruction. In this case, due to memory limitations and to keep the computational time rather small, we have computed only 15 iterations of SGD with a batch size of 300 and a learning rate of 0.5. In figure 13 we see that the loss functional rapidly decays over the iterations of the SGD algorithm. In the plot at the right, we see the evolution of the error of our reconstructed point clouds with respect to the ground truth (see formulae (3.6) and (3.7)). As before, we have used the PyTorch implementation of the SGD algorithm. This time, it took around 10 minutes to compute 15 iterations in a MacBook Pro 1.4 GHz Intel Core i5 with 16 GB of RAM memory. See figure 14 for some example of the tomographic reconstructions of the 3D structures presented in this subsection.

APPENDIX A. DISCRETE FRENET FRAMES

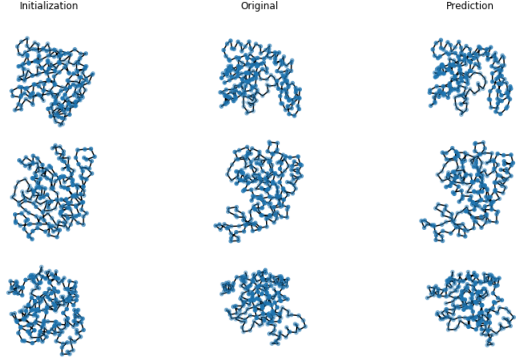
In this section, we check that any atomic structure (point cloud $\{z_1, z_2, \dots, z_m\} \in \mathbb{R}^{3m}$) satisfying the discrete curve property

$$(A.1) \quad \exists \delta > 0 \quad \text{such that} \quad \|z_{j+1} - z_j\| = \delta, \quad \forall j \in \{1, \dots, m-1\},$$

where $\{z_1, z_2, \dots, z_m\}$ are the positions of the atoms in the molecular structure, can be represented by the parameters $(\Theta, \Psi, \hat{z}, \hat{F})$ introduced in subsection 2.1. The construction of the discrete curve



(A) Clean 2D tomographic projections of the reconstructed 3D structures. At the left we see the structure in the given conformation, in the middle the ground true and at the right the reconstruction.



(B) At the left we see the structure in the known conformation (after a random rotation), in the middle we see the particle in its specific conformation (ground truth) and at the right the 3D atomic structure predicted by means of our method.

FIGURE 14. Some examples of the tomographic reconstruction of three-dimensional structures from tomographic projections.

using this parameters is based on a discrete version of the Frenet Frames, which is extensively used in the description of smooth curves, and we use the same approach and notation as in [10]. This representation of the atomic structure, in which the parameters (\hat{z}, \hat{F}) represent the spatial location and the orientation of the structure and the parameters (Θ, Ψ) represent the shape of the discrete curve up to translations and rotations is crucial in our approach. Although this representation of discrete curves by using the torsion and bond angles is standard and can be found in many works, we include it here for completeness.

As mentioned in subsection 2.1, we need to select a reference atom $j_0 \in \{1, \dots, m-1\}$ (a reference point in the discrete curve), which will serve as initial condition to construct the rest of the point cloud. This choice is arbitrary, but it is preferable to select an atom from a non-flexible part of the molecule (a part of the structure invariant over the different conformations).

Let us define the map

$$(A.2) \quad \begin{aligned} \mathbf{Z}: \quad \mathcal{A} \times \mathcal{I} &\longrightarrow \mathbb{R}^{3m} \\ (\Theta, \Psi, \hat{z}, \hat{F}) &\longmapsto \mathbf{Z}(\Theta, \Psi, \hat{z}, \hat{F}), \end{aligned}$$

where $\mathbf{Z}(\Theta, \Psi, \hat{z}, \hat{F}) = \{z_1, z_2, \dots, z_m\} \in \mathbb{R}^{3m}$ is the solution to the dynamical system

$$(A.3) \quad \begin{cases} z_{j+1} = z_j + \delta e_3 F_j & j \in \{1, \dots, m-1\} \\ F_j = R(\theta_j, \psi_j) F_{j-1} & j \in \{2, \dots, m-2\} \\ \text{with } z_{j_0} = \hat{z} \in \mathbb{R}^3 \text{ and } F_{j_0} = \hat{F} \in SO(3), \end{cases}$$

with $\delta > 0$ fixed, $e_3 = (0, 0, 1)$ and $R(\theta_j, \psi_j) \in SO(3)$ being the rotation matrix

$$(A.4) \quad R(\theta_j, \psi_j) = \begin{pmatrix} \cos \psi_j \cos \theta_j & \cos \psi_j \sin \theta_j & -\sin \psi_j \\ -\sin \theta_j & \cos \theta_j & 0 \\ \sin \psi_j \cos \theta_j & \sin \psi_j \sin \theta_j & \cos \psi_j \end{pmatrix},$$

with $\Theta = (\theta_2, \theta_3, \dots, \theta_{m-1})$ and $\Psi = (\psi_2, \psi_3, \dots, \psi_{m-1})$. We recall the abbreviated notation $\mathcal{A} := [-\pi, \pi]^{m-2} \times [-\pi, \pi]^{m-2}$ and $\mathcal{I} := \mathbb{R}^3 \times SO(3)$ that we already used in subsection 2.1.

It is not difficult to see that the image of \mathbf{Z} is contained in the set of point clouds $\{z_1, \dots, z_m\} \in \mathbb{R}^{3m}$ satisfying (A.1). Next we prove that the map \mathbf{Z} is indeed onto, i.e., any point cloud satisfying (A.1) can be represented as $\mathbf{Z}(\Theta, \Psi, \hat{z}, \hat{F})$. Although this result is well-known, we include it here for completeness and also to show the construction and notation of the discrete Frenet frames that we use throughout the paper.

Lemma A.1. *Let $m \in \mathbb{N}$ and $\delta > 0$, and let $\{z_1, z_2, \dots, z_m\} \in \mathbb{R}^{3m}$ be any point cloud satisfying (A.1). Then, there exist $(\Theta, \Psi, \hat{z}, \hat{F}) \in \mathcal{A} \times \mathcal{I}$ such that $\mathbf{Z}(\Theta, \Psi, \hat{z}, \hat{F}) = \{z_1, z_2, \dots, z_m\}$.*

Proof. We use the same construction of the discrete Frenet Frames as in [10]. Let $\{z_1, \dots, z_m\} \in \mathbb{R}^{3m}$ be a point cloud satisfying (A.1) for some given $\delta > 0$. We need to compute the Frenet Frames at every point z_j for $j \in \{1, \dots, m-1\}$. First we compute the sequence of unitary vectors $\mathbf{T} := \{t_j\}_{j=1}^{m-1}$ given by

$$t_j = \frac{z_{j+1} - z_j}{\delta}, \quad \forall j \in \{1, \dots, m-1\}.$$

These are the directions of each segment in the discrete curve. Next, we compute the sequence of binormal vectors $\mathbf{B} := \{b_j\}_{j=1}^{m-1}$, given by

$$(A.5) \quad b_j = \frac{t_{j-1} \times t_j}{|t_{j-1} \times t_j|} \quad \forall j \in \{2, \dots, m-1\} \quad \text{and} \quad b_1 = b_2,$$

and the sequence of normal vectors $\mathbf{N} := \{n_j\}_{j=0}^{m-1}$ as

$$n_j = b_j \times t_j, \quad \forall j \in \{1, \dots, m-1\}.$$

Finally we define the sequence of Frenet frames as $\mathbf{F} := \{F_j\}_{j=1}^{m-1}$, where each frame $F_j \in SO(3)$ is the 3×3 matrix that has n_j , b_j and t_j as rows, i.e.

$$(A.6) \quad F_j := \begin{bmatrix} n_j \\ b_j \\ t_j \end{bmatrix}, \quad \forall j \in \{1, \dots, m-1\}.$$

Given the sequence of $m-1$ Frenet frames $\mathbf{F} := \{F_j\}_{j=1}^{m-1}$, we can compute the sequence of $m-2$ rotation matrices $\mathbf{R} := \{R_j\}_{j=2}^{m-1}$ given by

$$(A.7) \quad R_j := F_{j+1} F_j^* \quad \forall i \in \{2, \dots, m-2\}.$$

One can readily prove that the sequence $\{z_1, z_2, \dots, z_m\}$ satisfies

$$\begin{cases} z_{j+1} = z_j + \delta e_3 F_j & j \in \{1, \dots, m-1\} \\ F_j = R_j F_{j-1} & j \in \{2, \dots, m-2\}. \end{cases}$$

Using the same arguments as in [10, Section 3.B], each rotation matrix $R_j \in \mathbf{R}$, constructed as in (A.6)–(A.7), is given by $R_j = R(\theta_j, \psi_j)$ defined in (A.4), where $\theta_j \in [-\pi, \pi]$ is the torsion angle

$$\cos \theta_j = b_{j+1} \cdot b_j,$$

and $\psi_j \in [0, \pi]$ is the bond angle, and satisfies

$$\cos \psi_j = t_{j+1} \cdot t_j.$$

Note that, in view of (A.5), we have $\theta_1 = 0$.

Hence, given any sequence of m points $\{z_1, z_2, \dots, z_m\} \in \mathbb{R}^{3m}$ satisfying (A.1), we can compute the associated sequence of torsion and bond angles $[\Theta, \Psi] \in \mathcal{A}$, which along with the position \hat{z} and the orientation \hat{F} of the curve at the j_0 -th atom yield $\mathbf{Z}(\Theta, \Psi, \hat{z}, \hat{F}) = \{z_1, \dots, z_m\}$. \square

APPENDIX B. MANIFOLD SPECTRAL REPRESENTATION

In this section, we describe the method to construct the graph Laplacian, from the cryo-EM dataset, which is used in subsection 2.2 to approximate the spectral properties of the unknown manifold of conformations \mathcal{M} . As outlined in [17], the low-resolution reconstruction of the heterogeneous particles in the dataset obtained by the method in [2] can be used to construct a weighted graph. Each vertex in the graph corresponds to a particle in the dataset, and the weights in the edges joining any two vertices are estimates of the affinity between the low-dimensional reconstructions of the 3D densities (i.e. the similarity between the underlying conformation of the particles).

Let us choose $N' < N$, where $N \times N$ is the resolution in pixels of the cryo-EM images and $N' \times N' \times N'$ is the resolution of the voxel representation of the 3D densities that we aim to reconstruct. As indicated in [17, Subsection 3.3], this method is limited to a low-resolution reconstruction, i.e. $N' \ll N$. In [2], the volume density associated to each particle $\hat{U}_i \in \mathbb{R}^{N' \times N' \times N'}$ is estimated as

$$\hat{U}_i = \hat{\mu} + \hat{V}_q \beta_i,$$

where $\hat{\mu} \in \mathbb{R}^{N' \times N' \times N'}$ is the estimated average density, $\hat{V}_q \in [\mathbb{R}^{N' \times N' \times N'}]^q$ is a tensor with the q principal components of the estimated covariance matrix $\hat{\Sigma}$ (the so-called eigenvolumes) and $\beta_i \in \mathbb{R}^q$ are the PCA coefficients associated to the i -th particle. Here, the volumes \hat{U}_i are reconstructed independently of the viewing direction of each particle, and then, the PCA components β_i depend only on the conformation of the underlying particle. They can actually be used as a low-dimensional representation of the underlying conformation. In view of the second part of Assumption 1, these PCA coefficients $\beta_i \in \mathbb{R}^q$ can be seen as a discrete approximation of a d -dimensional manifold $\mathcal{M} \subset \mathbb{R}^q$, with $d < q$.

We stress that any dimensionality reduction of the three-dimensional structures of the particles might be used, instead of the PCA coefficients, for the construction of the graph. We only need that the low-dimension representations of the volumes are invariant under rotations and translations. For instance, the representation of the particles in the latent space obtained by a trained variational auto-encoder [23, 31] may work as well.

We now construct a weighted graph using the low-dimension representation of the conformation in each particle, denoted by $\beta_i \in \mathbb{R}^q$. The weight W_{ij} between any two vertices i and j in the graph

must represent the similarity between the underlying conformations of the particles i and j . In the numerical experiments presented in section 3, we used a Gaussian kernel weights of the form

$$W_{ij} = \exp \left[\frac{-\|\beta_i - \beta_j\|^2}{2\sigma^2} \right],$$

for some $\sigma > 0$ fixed. It is well-known that the computational complexity to compute the eigenvectors of a graph Laplacian can be significantly reduced when the associated matrix is sparse. This can be achieved by setting to 0 all the weights W_{ij} below a certain threshold. In the numerical experiments in subsection 3, due to the rather small size of the synthetic datasets (only 4000 images), we could use a dense matrix of similarities.

Another possibility is to consider binary weights obtained by applying a symmetric k Nearest Neighbours (KNN),

$$W_{ij} := \begin{cases} 1, & \text{if } \beta_i \in NN_k(\beta_j) \text{ or } \beta_j \in NN_k(\beta_i) \\ 0 & \text{otherwise,} \end{cases}$$

where $\beta_i \in NN_k(\beta_j)$ means that β_i is one of the k nearest neighbours of β_j . This choice provides a sparse matrix of similarities, which may increase the computational efficiency when computing the eigenvectors of the graph Laplacian.

Once we have constructed the matrix of similarities between the conformations of the particles in the cryo-EM dataset, we need to define an associated Laplacian. In our numerical experiments we have used the symmetric normalized graph Laplacian, defined as

$$L := D^{-1/2}(D - W)D^{-1/2},$$

where D is the degree matrix, i.e. the diagonal matrix with entries given by $D_{ii} = \sum_{j=1}^n W_{ij}$. Finally, the eigenvectors (2.5) are obtained as the eigenvectors of L associated to the K smallest eigenvalues.

REFERENCES

- [1] J. Andén, E. Katsevich, and A. Singer. Covariance estimation using conjugate gradient for 3D classification in cryo-EM. In *2015 IEEE 12th International Symposium on Biomedical Imaging (ISBI)*, pages 200–204. IEEE, 2015.
- [2] J. Andén and A. Singer. Structural variability from noisy tomographic projections. *SIAM Journal on Imaging Sciences*, 11(2):1441–1492, 2018.
- [3] A. Barnett, L. Greengard, A. Pataki, and M. Spivak. Rapid solution of the cryo-EM reconstruction problem by frequency marching. *SIAM Journal on Imaging Sciences*, 10(3):1170–1195, 2017.
- [4] O. Beckstein, S. L. Seyler, and A. Kumar. Simulated trajectory ensembles for the closed-to-open transition of adenylate kinase from DIMS MD and FRODA. 10 2018.
- [5] M. Berger, P. Gauduchon, and E. Mazet. Le spectre d’une variété riemannienne. *Le Spectre d’une Variété Riemannienne*, pages 141–241, 1971.
- [6] Y. Cheng, N. Grigorieff, P. A. Penczek, and T. Walz. A primer to single-particle cryo-electron microscopy. *Cell*, 161(3):438–449, 2015.
- [7] J. Frank. *Three-dimensional electron microscopy of macromolecular assemblies: visualization of biological molecules in their native state*. Oxford university press, 2006.
- [8] T. Grant, A. Rohou, and N. Grigorieff. cisTEM, user-friendly software for single-particle image processing. *elife*, 7:e35383, 2018.
- [9] D. S. Grebenkov and B.-T. Nguyen. Geometrical structure of Laplacian eigenfunctions. *siam REVIEW*, 55(4):601–667, 2013.
- [10] S. Hu, M. Lundgren, and A. J. Niemi. Discrete Frenet frame, inflection point solitons, and curve visualization with applications to folded proteins. *Physical Review E*, 83(6):061908, 2011.

- [11] J. Jumper, R. Evans, A. Pritzel, T. Green, M. Figurnov, O. Ronneberger, K. Tunyasuvunakool, R. Bates, A. Žídek, A. Potapenko, et al. Highly accurate protein structure prediction with AlphaFold. *Nature*, 596(7873):583–589, 2021.
- [12] E. Katsevich, A. Katsevich, and A. Singer. Covariance matrix estimation for the cryo-EM heterogeneity problem. *SIAM journal on imaging sciences*, 8(1):126–185, 2015.
- [13] A. B. Lee and R. Izbicki. A spectral series approach to high-dimensional nonparametric regression. *Electronic Journal of Statistics*, 10(1):423–463, 2016.
- [14] H. Y. Liao and J. Frank. Classification by bootstrapping in single particle methods. In *2010 IEEE International Symposium on Biomedical Imaging: From Nano to Macro*, pages 169–172. IEEE, 2010.
- [15] D. Lyumkis, A. F. Brilot, D. L. Theobald, and N. Grigorieff. Likelihood-based classification of cryo-EM images using frealign. *Journal of structural biology*, 183(3):377–388, 2013.
- [16] J. L. Milne, M. J. Borgnia, A. Bartesaghi, E. E. Tran, L. A. Earl, D. M. Schauder, J. Lengyel, J. Pierson, A. Patwardhan, and S. Subramaniam. Cryo-electron microscopy—a primer for the non-microscopist. *The FEBS journal*, 280(1):28–45, 2013.
- [17] A. Moscovich, A. Halevi, J. Andén, and A. Singer. Cryo-EM reconstruction of continuous heterogeneity by Laplacian spectral volumes. *Inverse Problems*, 36(2):024003, 2020.
- [18] P. A. Penczek. Variance in three-dimensional reconstructions from projections. In *Proceedings IEEE International Symposium on Biomedical Imaging*, pages 749–752. IEEE, 2002.
- [19] P. A. Penczek, M. Kimmel, and C. M. Spahn. Identifying conformational states of macromolecules by eigenanalysis of resampled cryo-EM images. *Structure*, 19(11):1582–1590, 2011.
- [20] P. A. Penczek, C. Yang, J. Frank, and C. M. Spahn. Estimation of variance in single-particle reconstruction using the bootstrap technique. In *Single-Particle Cryo-Electron Microscopy: The Path Toward Atomic Resolution: Selected Papers of Joachim Frank with Commentaries*, pages 389–404. World Scientific, 2006.
- [21] A. Punjani, J. L. Rubinstein, D. J. Fleet, and M. A. Brubaker. cryoSPARC: algorithms for rapid unsupervised cryo-EM structure determination. *Nature methods*, 14(3):290–296, 2017.
- [22] L. Rosasco, M. Belkin, and E. De Vito. On learning with integral operators. *Journal of Machine Learning Research*, 11(2), 2010.
- [23] D. Rosenbaum, M. Garnelo, M. Zielinski, C. Beattie, E. Clancy, A. Huber, P. Kohli, A. W. Senior, J. Jumper, C. Doersch, et al. Inferring a continuous distribution of atom coordinates from cryo-EM images using VAEs. *arXiv preprint arXiv:2106.14108*, 2021.
- [24] S. H. Scheres. A Bayesian view on cryo-EM structure determination. *Journal of molecular biology*, 415(2):406–418, 2012.
- [25] S. H. Scheres. RELION: implementation of a Bayesian approach to cryo-EM structure determination. *Journal of structural biology*, 180(3):519–530, 2012.
- [26] K. Tunyasuvunakool, J. Adler, Z. Wu, T. Green, M. Zielinski, A. Žídek, A. Bridgland, A. Cowie, C. Meyer, A. Laydon, et al. Highly accurate protein structure prediction for the human proteome. *Nature*, 596(7873):590–596, 2021.
- [27] M. Varadi, S. Anyango, M. Deshpande, S. Nair, C. Natassia, G. Yordanova, D. Yuan, O. Stroe, G. Wood, A. Laydon, et al. AlphaFold Protein Structure Database: massively expanding the structural coverage of protein-sequence space with high-accuracy models. *Nucleic acids research*, 50(D1):D439–D444, 2022.
- [28] K. R. Vinothkumar and R. Henderson. Single particle electron cryomicroscopy: trends, issues and future perspective. *Quarterly reviews of biophysics*, 49, 2016.
- [29] U. Von Luxburg, M. Belkin, and O. Bousquet. Consistency of spectral clustering. *The Annals of Statistics*, pages 555–586, 2008.
- [30] M. Vulović, R. B. Ravelli, L. J. van Vliet, A. J. Koster, I. Lazić, U. Lüken, H. Rullgård, O. Öktem, and B. Rieger. Image formation modeling in cryo-electron microscopy. *Journal of structural biology*, 183(1):19–32, 2013.
- [31] E. D. Zhong, T. Bepler, B. Berger, and J. H. Davis. CryoDRGN: reconstruction of heterogeneous cryo-EM structures using neural networks. *Nature methods*, 18(2):176–185, 2021.